A Skeletal Kinetic Mechanism for PRF Combustion in HCCI Engines

Patrick Kirchen, Mahdi Shahbakhti, Charles Robert Koch*

Department of Mechanical Engineering
4-9 Mechanical Engineering, University of Alberta
Edmonton, Alberta, Canada, T6G 2G8
Tel: (780) 492-8821, Fax: (780) 492-2200

Abstract

A single zone thermodynamic model, coupled to a kinetic mechanism, is developed and is capable of predicting the ignition timing of Primary Reference Fuels (PRFs) in a Homogeneous Charge Compression Ignition (HCCI) engine. A new combination of kinetic mechanisms is used, which includes 120 reactions and 58 species for both ignition and high temperature reactions. The model is validated using a step by step methodology. The validation compares ignition delays predicted by the model with published measurements from a rapid compression machine, shock tube as well as the cylinder pressure histories taken from two different experimental HCCI engines for various operating conditions. The model is able to qualitatively predict the effect of different parameters such as gas temperature, gas pressure, equivalence ratio and octane number on the HCCI ignition delay.

Keywords: Internal Combustion Engines, Ignition, HCCI, Primary Reference Fuel, Kinetic Modeling

1 Introduction

The Homogeneous Charge Compression Ignition (HCCI) engine holds the potential for Diesel like fuel efficiency with low NOx and low particulate emissions (Onishi et al. 1979), (Najt and Foster 1983), (Lavy et al. 2000). As in a Spark Ignited (SI) engine, a homogeneous air/fuel mixture is drawn into the cylinder and compressed. Ignition of the mixture does not depend on a spark but rather on the compression of the mixture,

* Corresponding author

through which the temperature and pressure of the mixture are such that it will autoignite. The ignition process is the major obstacle in implementing the HCCI cycle as there is no distinct control mechanism available for the combustion timing (Tunestal et al. 2002). From early in HCCI research it has been accepted that the combustion process is governed by chemical kinetics (Najt and Foster 1983), and hence influenced by many parameters. The most dominant of these parameters are the fuel reactivity (describable in terms of the octane number, ON), and the temperature and pressure history of the mixture, which are both affected by other engine parameters.

While experimental research is essential in understanding the HCCI cycle, chemical kinetic modeling is invaluable for not only furthering the understanding of this cycle, but also for carrying out investigations that would prove to be too laborious or expensive to carry out experimentally. Chemical kinetic mechanisms for the ignition and combustion of the Primary Reference Fuels (PRF), n-heptane and iso-octane, have ranged from simple, general kinetic mechanisms (Halstead et al. 1977), (Hu and Keck 1987), (Tanaka et al. 2003) to complex, detailed mechanisms (Curran et al. 1998), (Curran et al. 2002), (Slavinskaya and Haidn 2003). Detailed mechanisms provide much of the understanding of the underlying physical processes in the ignition and combustion process, but are often too computationally expensive to implement for heavier hydrocarbons or when many simulations are required. Simplified mechanisms have lower computational requirements, but are limited to only the operating parameters for which they were developed.

Chemical kinetic mechanisms coupled with thermodynamic models lend themselves well to the development of HCCI control systems and control strategies, as they are capable of predicting the ignition and combustion events without actually having to obtain experimental data for all operation points. Furthermore, it becomes possible to evaluate control systems without subjecting an engine to undue loads. Simplified mechanisms will help ease the development of such control systems for the HCCI engine without excessive computational requirements. Thus, a single zone model can be used to develop control strategies of HCCI ignition timing with modest computational resources.

In this investigation, a kinetic mechanism describing the ignition and combustion of primary reference fuels is developed and coupled with a one-zone thermodynamic model with the main goal of predicting the

effect of engine parameters on the ignition timing. The ability to predict the effect of these parameters is a valuable tool for the development of HCCI control strategies, and a one zone model is well suited to this task as only general, qualitative dependencies are required. The model is validated against experimental data taken from a Rapid Compression Machine (RCM), a shock tube, and two experimental HCCI engines. As well, a comparison with theoretically determined combustion temperatures and equilibrium compositions is used to validate the model's ability to predict equilibrium conditions.

2 Theory

A one zone thermodynamic model coupled to a chemical kinetic mechanism is used to approximate the combustion process in several practical systems. A brief overview of both the thermodynamic model and its components, as well as the kinetic mechanism is presented below.

2.1 Thermokinetic Model

A one zone thermodynamic model, with the assumption of a spatially uniform thermodynamic state within the combustion chamber, is used for this investigation as it has only modest computational requirements. The gas temperature, pressure, and composition are assumed to be spatially uniform throughout the combustion chamber. In addition, the mixture is assumed to be one of ideal gases with a constant mass (i.e. no blowby).

The variation of the thermodynamic state of the mixture with time is described through a first law analysis of the system shown in Figure 1:

$$\frac{dU}{dt} = \dot{W} + \frac{dQ}{dt} \tag{1}$$

Where $\frac{dU}{dt}$ is the variation of the internal energy with time, $\dot{W}$ is the mechanical work added to the system, and $\frac{dQ}{dt}$ is energy added to the system. For a variable volume system, the mechanical work can be represented using:

$$\dot{W} = -P\frac{dV}{dt} \tag{2}$$

Following the assumption that the system is closed, $\frac{dQ}{dt}$ is only due to heat transfer. The change in

internal energy is due to changes in the mixture composition and temperature and can be described as follows:

$$\frac{dU}{dt} = \sum_i \frac{dN_i}{dt}\bar{h}_i - RT\sum \frac{dN_i}{dt} + \frac{dT}{dt}\left(\sum_i N_i \bar{c}_{p,i} - N_{mix}R_u\right) \tag{3}$$

Where N_i is the number of moles of the i^{th} species, N_{mix} is the number of moles in the mixture, $\bar{h}_i$ is the molar specific enthalpy of the i^{th} species, R_u is the universal gas constant, and $\bar{c}_{p,i}$ is the molar specific heat of the i^{th} species. Equation 3 can be combined with equation 1 and rearranged to give the rate of change of the mixture temperature.

$$\frac{dT}{dt} = \frac{-P\frac{dV}{dt} - \frac{dQ}{dt} - \sum_i \frac{dN_i}{dt}\bar{h}_i + R_u T\sum_i \frac{dN_i}{dt}}{\sum_i N_i \bar{c}_{p,i} - N_{mix}R_u} \tag{4}$$

The heat transfer to the cylinder walls, $\frac{dQ}{dt}$, is modeled using the Woschni heat transfer correlation, which provides an estimate of the overall heat transfer coefficient based on the in-cylinder conditions (Woschni 1967):

$$h_{wall} = \alpha_{scaling} B^{-0.2} P^{0.8} T^{-0.53} \left(2.28\bar{S}_p\right)^{0.8} \tag{5}$$

where h_{wall} is the overall heat transfer coefficient [W/(m^{2}K)], B is the cylinder bore [m], P is the instantaneous cylinder pressure [kPa], T is the mixture temperature [K], and $\bar{S}_p$ is the mean piston speed [m/s].

As the Woschni heat transfer correlation is based on measurements from a diesel engine, a scaling factor $\alpha_{scaling}$ is used for tuning of the correlation to match a specific engine geometry (Woschni 1967, Chang et al. 2004). Due to the sooting and diffusion type flame in diesel combustion, the Woschni correlation will have higher radiative heat transfer components than an HCCI combustion event (Fiveland and Assanis 2000), leading to $\alpha_{scaling}$ being smaller for an HCCI engine. It should also be noted that typically the contribution of the combustion event to the heat transfer is considered using an additional term which is not present in equation 5. This term accounts for the fluid motion from the density change of the mixture due to the flame front. However, since HCCI does not have a distinct flame front and the

mixture is assumed to combust uniformly, this term is not included in this investigation.

The temporal variation of the mixture composition, $\frac{dN_i}{dt}$, is described using a chemical kinetic mechanism. For a system of *J* reactions and *I* species the law of mass action is used to describe the rate of change of concentration of each chemical species with an ordinary differential equation of the form:

$$\frac{d[C_i]}{dt} = \sum_{j=1}^{J}\left(\left[\nu''_{i,j} - \nu'_{i,j}\right] \times k_{f,j} \prod_{i=1}^{I} \left([C_{i,j}]^{\nu'_{i,j}} \right) \right) \tag{6}$$

where the forward Arrehenius rate of the j[th] reaction, k_{fj}, is defined by:

$$k_{f,j} = AT^n e^{\frac{-Ea}{R_u T}} \tag{7}$$

where *i* is the species index, *j* is the reaction index, $\nu''_{i,j}$ and $\nu'_{i,j}$ are the stoichiometric coefficients of the i^{th} species in the j^{th} reaction on the product and reactant sides, respectively, $[C_{i,j}]$ is the concentration of the i^{th} species in the j^{th} reaction, *A* and *n* are constants, E_a is the activation energy, and *T* is the mixture temperature. Depending on the reaction being considered, the reverse reaction rate, k_b, may be relevant and is determined using the equilibrium constant, K_{eq}:

$$K_{eq} = \frac{k_f}{k_b} \tag{8}$$

Unless reverse reaction rates are explicitly specified in the literature, they are calculated using the equilibrium constant. The reaction rates for unimolecular reactions are adjusted to account for low pressure fall off and third body collision efficiencies, where required.

Whenever possible, the thermodynamic properties are determined using the NASA polynomials taken from the Burcat (2001) database. When this is not possible, generally in the case of fuel-based radicals, the properties are estimated using additivity rules as is traditionally done, for example by Zheng et al. (2002) or Slavinskaya and Haidn (2003) [1]. More specifically, the NIST (Stein and Brown 2003) implementation of the Benson (1976) additivity rules are used to estimate the specific heat from 300K to ~ 1000K, as well as the absolute entropy and enthalpy at 298K. The specific heats are then extrapolated to

[1] Properties were estimated for the following species: C_3H_7CHO, $C_7H_{15}OO$, C_3H_7CHO, $C_3H_7O_2$, C_3H_7OOH, $C_7H_{14}O$, $C_7H_{14}OOH$, $C_7H_{14}OOH$, $C_7H_{15}OO$, $C_7H_{15}OOH$, $C_8H_{16}O$, $C_8H_{16}OOH$, $C_8H_{17}O$, $C_8H_{17}OO$, $C_8H_{17}OOH$, $OC_7H_{13}O$, $OC_7H_{13}OOH$, $OC_8H_{15}O$, $OC_8H_{15}OOH$, $OOC_7H_{14}OOH$, $OOC_8H_{16}OOH$.

5000K using the Wilhoit polynomials (Burcat 1984) and fit to the NASA polynomials using a least squares regression.

2.2 Kinetic Mechanism

Recently, several kinetic mechanisms geared towards the HCCI combustion of PRFs have been presented, each with its associated advantages and disadvantages. Zheng et al. (2002) presented a mechanism using the ignition chemistry based on Li et al. (1996), combined with the intermediate and high temperature chemistry of Griffiths et al. (1994). The PRF blend is treated as a single fuel molecule with its own associated reaction rate parameters. Different PRF's, and hence octane numbers, then have different rate parameters which must be determined for each fuel. This can be avoided by including separate fuel specific reactions for the ignition process, as is done by Tanaka et al. (2003), and then treating the subsequent oxidation process indiscriminately for the two fuels (Warnatz 2000). This has the disadvantage that more differential equations, in the form of equation 6, must be solved.

The higher temperature processes can be represented by either a set of global reactions, as done by Tanaka et al. (2003), or with more fundamental reactions as done by Zheng et al. (2002) (based on Griffiths et al. (1994)). The disadvantage of global reactions is that the conditions for which they are valid must be well known, and caution should be used when implementing them for extrapolative purposes. They do however have the advantage of reducing the mechanism size and hence the computational requirements.

In this study, a chemical kinetic mechanism with 102 reactions and 58 species is developed to describe the autoignition and oxidation of PRF's. A schematic of the general form of the mechanism is shown in Figure 2, while the complete mechanism is given in Table 7. The mechanism presented by Zheng et al. (2002) is modified to include both PRFs, rather than just the blended fuel, making it possible to consider the effects of different octane numbers without having to determine new reaction rates. Fuel specific rates are taken from Li et al. (1996) and used for the isomerization (R5, R6, R31, R32), and ether formation (R25 and R50) reactions[2]. A fuel interaction reaction is included as it was found by Tanaka et al. (2003) to improve the prediction of ignition delays for PRFs:

[2] R# refers to the reaction number in the mechanism given in the appendix.

$$C_8H_{18} + C_7H_{15} \Leftrightarrow C_7H_{16} + C_8H_{17} \quad \text{(R64)}$$

The H_2/O_2 sub mechanism presented by Marinov et al. (1995) is included as this mechanism will be used for future combustion investigations that include hydrogen as a fuel. The CO oxidation chemistry is described using the following reactions taken from Tanaka et al. (2003) and the rates from Smith et al. (2004):

$$CO+OH \Leftrightarrow CO_2 + H \quad \text{(R99)}$$

$$CO+HO_2 \Leftrightarrow CO_2 + OH \quad \text{(R100)}$$

$$CO+O+M \Leftrightarrow CO_2 + M \quad \text{(R101)}$$

$$CO+O_2 \Leftrightarrow CO_2 + O \quad \text{(R102)}$$

A more detailed discussion of the thermodynamic model and chemical kinetic mechanism is presented in Kirchen (2004).

3 Model Validation

The thermokinetic model is first validated based on its ability to predict combustion temperatures and equilibrium compositions for a constant volume combustion event. Ignition delay predictions are then compared to measured values taken from a shock tube and an RCM for various PRF's. Finally, the pressure histories from two single cylinder experimental engines running in HCCI mode are compared to the pressure histories predicted by the model. Each of these validations is discussed in greater detail below.

3.1 Equilibrium Validation

The ability of the model to predict the adiabatic combustion temperature and equilibrium product composition of a constant volume combustion event is validated using STANJAN (Reynolds 1987). STANJAN, given the initial thermodynamic state of a mixture, determines the final thermodynamic state of the mixture (composed of user specified species), based on the minimization of Gibbs Energy. Equilibrium compositions based on the minimization of Gibbs Free Energy and the solution of a kinetic mechanism should be the same given that (Come 2001): 1) all pertinent reactions are included in the mechanism; 2) accurate reaction rates (both forward and reverse) are used; and 3) the kinetic mechanism is solved over a sufficiently long time such that steady state conditions are reached.

Simulations are carried out using a constant volume combustion chamber with 20PRF and equivalence ratios ranging from Φ = 0.5 to 1.0. For each of these mixtures, an initial temperature of 800K and an initial pressure of 30 bar are specified. These conditions are used as they are indicative of the in-cylinder conditions at Top Dead Center (TDC) of an engine operating in HCCI mode. The same initial conditions are specified to both STANJAN and the thermokinetic model, after which the equilibrium thermodynamic state is determined. In order to ensure that thermokinetic model has converged to steady state equilibrium conditions, each simulation is carried out for 10 seconds. Heat transfer is not considered for the simulations using the thermokinetic calculations, as the combustion process is assumed to be adiabatic.

The adiabatic combustion temperatures calculated by the thermokinetic model and STANJAN are compared in Figure 3. After sufficient time, the temperatures predicted by the thermokinetic model (denoted by the heavy lines) approach those predicted by STANJAN (denoted by the thin horizontal lines). Combustion temperatures calculated using the thermokinetic model are in general agreement with those determined using STANJAN. For all equivalence ratios, the combustion temperature is under predicted, with a maximum error of 8.5% at stoichiometric conditions. The concentration of the major exhaust gas constituents (i.e. CO_2, H_2O, O_2, and N_2) are predicted with a mean error of 8.6%

This investigation validates the ability of the model to predict the combustion temperatures and equilibrium compositions. This does not necessarily ensure that chemical kinetic mechanism will predict the combustion emissions, as the emissions from an HCCI engine are strongly influenced by both the temporal and spatial variations of the in-cylinder temperature and species concentration distributions.

3.2 Ignition Delay Validation

One of the primary uses of chemical kinetic modeling in HCCI research is to predict the autoignition timing, which is crucial for HCCI engine operation. Published experimental ignition delay measurements from both a Rapid Compression Machine (RCM) and a shock tube are used to validate the kinetic mechanism.

3.2.1 RCM Validation

The experimental RCM ignition delay measurements presented by Park and Keck (1990) are used to

validate the ability of the thermokinetic model to predict the ignition delays in a practical combustion system. It is assumed that the compression process is sufficiently fast that the kinetic activity during the compression stroke is negligible. Thus, the compression stroke is not considered for the simulations and the compressed state of the mixture is modeled at a constant volume. Simulation initial conditions are taken as the end of compression conditions from the experiments and are given in Table 1. Ignition delays are calculated using the thermokinetic model for each of the conditions given in Table 1 with stoichiometric air/fuel mixtures of different five fuel blends (0PRF, 50PRF, 75PRF, 90PRF, 100PRF).

Heat transfer is neglected for the RCM validation as the RCM piston contains a crevice volume in which the roll up vortices formed during compression are contained, thus significantly reducing the convective heat transfer (Park and Keck 1990). Furthermore, Griffiths et al. (1993) have found that it is reasonable to neglect heat transfer in RCM simulations as the core temperature remains relatively unaffected by the wall heat transfer prior to ignition.

Park and Keck define the measured ignition delay as being the time from the inflection point in the pressure during compression (indicative of the end of compression), to the time at which the mixture temperature exceeds 1100K. The simulation ignition delay is defined in a similar fashion as being the time from the beginning of the simulation (end of compression), to the point at which the mixture temperature exceeds 1100K. Both of these methods represent the time from the end of compression to the high temperature ignition process.

A comparison of the simulated and measured ignition delays is given in Figure 4, in which the symbols indicate measured ignition delays from Park and Keck and the lines indicate simulation results. The thermokinetic model is able to qualitatively predict the effects of temperature (plotted in Arrhenius form on the abscissa), pressure (denoted by the hollow and filled symbols) and octane number (denoted by different symbols) on the ignition delays (shown on the ordinate). The ignition delays of n-heptane, while qualitatively correct, are under-predicted for all conditions. In order to further examine this, the ability of the thermokinetic model to predict ignition delays in a shock tube is validated for n-heptane.

3.2.2 Shock Tube Validation

In order to ensure that the mechanism is indeed capable of predicting the physical process of autoignition, a second ignition delay validation with shock tube data is carried out. In particular, the experimental ignition delays (Gauthier et al. 2004) are compared to those determined by the thermokinetic model. The shock tube validation is only carried out for stoichiometric mixtures of n-heptane at 20 bar for temperatures ranging from 800-1050K, in order to understand the difference between the measured and calculated ignition delays for n-heptane noted in the RCM validation. Again, the system is modeled as a constant volume, with the initial conditions for simulations taken from the state of the mixture after the passing of the shock wave. Due to the short time scales required for ignition to occur, heat transfer is neglected.

The ignition delay is defined as being the elapsed time from when the shock wave compresses the mixture to the time at which the rate of pressure rise is at a maximum. A comparison of the experimental and predicted ignition delays is given in Figure 5. As the figure shows, there is good agreement between the predicted and experimental ignition delays and the predicted values are within 0.5 ms of the experimental values.

3.3 HCCI Validation

In the previous equilibrium and ignition delay validations, the system is modeled as a constant volume process with initial conditions defined by the post compression mixture conditions from experiments. In the HCCI validation, the system is no longer modeled at a constant volume, as there is sufficient time during the compression stroke for slow chemical kinetic activity and heat transfer to take place. Experimental cylinder pressure traces taken from two different single cylinder engines running under HCCI mode are compared with those calculated by the thermokinetic model.

3.3.1 Engine Setup

Two different engines are used to carry out HCCI experiments. These are a Cooperative Fuels Research (CFR) single cylinder engine and a single cylinder Ricardo Mark III engine with a Rover A7

head. The geometry of each engine is given in Table 2. The experimental data for the CFR engine is taken from Atkins (2004) and Atkins and Koch (2005), while the experimental data for the Ricardo engine is briefly outlined in this investigation. A general schematic of the experimental apparatus for both engines is shown in Figure 6.

The premixed PRF blend is injected into the intake port and the exhaust gas composition is measured using Siemens and Horiba emissions analyzers. Fresh air entering the engine is heated by an air heater positioned upstream of the throttle body. The intake air heater is operated by a closed-loop controller to achieve a prescribed intake port air temperature. The controller uses the measured values of a temperature sensor located close to the intake port in the intake manifold. As this sensor measures the temperature of the combined intake air and EGR, this temperature includes the heating effect of EGR. The cylinder pressure is measured with a Kistler water-cooled ThermoCOMP (model 6043A60) piezoelectric pressure sensor that is flush mounted in the cylinder. The manufacturer indicates that the cylinder pressure thermal shock error or short time drift is less than 0.25 bar. The crank angle is measured by a BEI optical encoder with 0.1˚ resolution connected to the crankshaft on the front of the engine. The cylinder pressure and the encoder signals are measured with an MTS combustion analysis system, which provides real-time calculation of combustion and engine operating parameters. Exhaust gases are recirculated (EGR) using an insulated return line from the exhaust to the intake manifold. The recirculated exhaust gas fraction is determined by comparing the CO_2 concentrations in the intake and exhaust manifolds, and by assuming that all CO_2 in the intake manifold is from the exhaust gases.

3.3.2 Ignition point definition

In order to compare the calculated and experimental ignition timing, the point of ignition for both the experimental and calculated engine cycles are determined in the same fashion. A standard definition of ignition is the point at which the exothermicity of chemical reactions is greater than the energy lost to the environment (Glassman 1996). This definition could be used to determine the ignition timing from the simulation results as the heat transfer rate and reaction exothermicity are known quantities, but not for the experimental data as only the cylinder pressure is measured.

A method designed to detect engine knock from an SI engine pressure trace is adapted to detect autoignition in an HCCI engine. Checkel and Dale (1986) presented a robust method in which the onset of knock is characterized by a decrease in the third derivative of the pressure trace. This decrease corresponds to the rapid change of concavity of the pressure history from positive to negative during knocking. In HCCI engines it is the point at which the reaction exothermicity becomes substantial and begins to increase the cylinder pressure which must be detected. In the crank angle region near TDC during compression, the pressure history has a negative concavity, which becomes positive during ignition (i.e. a positive third derivative). By detecting this transition from negative to positive concavity, the point of ignition can be determined. In this investigation, ignition is defined as being the point at which the third derivative of the pressure trace with respect to the crank angle, θ, exceeds a heuristically determined limit:

$$\frac{d^3P}{d\theta^3} > \left.\frac{d^3P}{d\theta^3}\right|_{\lim} = 0.05 \quad \left[\frac{kPa}{CAD^3}\right] \tag{9}$$

It was found that if the ignition process is so slow that this algorithm does not detect it, the mixture does not go through the second ignition stage and is therefore not of interest. The limit was selected such that the point of ignition represented the change in concavity and was not affected by noise in the differentiated signal.

A major concern when differentiating numerically is the amplification of noise, as successive differentiation of the signal amplifies high frequency noise components. Both the experimental and simulated pressure traces were filtered using a fourth order Butterworth low pass filter to attenuate the high frequency noise which would have been amplified during differentiation. An experimentally determined cutoff frequency of $f_c = 0.278\text{CAD}^{-1}$ provided sufficient suppression of high frequency noise, without undue distortion of the pressure trace. As the pressure history was discretized at a constant angular rate (every 0.1CAD), the signal was filtered in the crank angle domain so that a constant f_c could be used for different engine speeds. Both the experimental and simulated pressure traces were filtered in the same manner to ensure that the ignition timings are indicative of the same phenomena.

3.3.3 Results

Simulations are started at the beginning of compression (i.e. Intake Valve Closing, IVC) and continue

until the exhaust valve opens. With the initial conditions given in Table 3, the thermokinetic model is run for the CFR engine. Three different PRF blends are used to validate the ability of the model to predict ignition timing for different octane numbers. Each of the three points corresponds to operation at approximately the same load (IMEP $\approx$5bar), but with distinctly different equivalence ratios and EGR rates. The mixture pressure at IVC, p_{ivc}, is taken from the experimental pressure trace and mixture temperature at IVC, T_{ivc}, is assumed to be in the vicinity of the measured temperature of EGR/air mixture[3].

Due to considerable piston blow-by in the CFR engine, the pressure during the compression stroke is over predicted by the thermokinetic model, and some means of compensating for this is required. The simulation compression ratio is reduced such that the simulated compression pressure for motored engine conditions match those measured in the engine. Suitable agreement is found by assuming a compression ratio of 11:1, rather than the geometric ratio of 12:1. This value is used for all subsequent simulations and not varied.

The calculated and simulated ignition timings for all three fuels are compared in Table 4, where the experimental results are from 50 consecutive engine cycles. Table 4 indicates that the model is capable of predicting the ignition timing for operation with different fuels, equivalence ratios, and EGR rates. The ignition timing predicted for the 40 and 60PRF cases are both within the range of the experimental data. In the case of 20PRF, ignition is predicted to occur 1.7 CAD earlier than the measured values, which may be attributed to an inaccurate initial temperature used for the simulation.

All the experimental HCCI points for the CFR engine (Atkins 2004) are at a constant intake temperature and a constant engine speed. To evaluate the performance of the model at different intake temperatures and engine speeds, measurements are taken using the Ricardo engine with the initial conditions listed in Table 5. This validation also evaluates the performance of the model when a different engine is considered.

In these validation points, the intake temperature varies from 58^{o}C to 144^{o}C, the equivalence ratio from 0.47 to 0.83, the EGR rate from 0% to 19.1%, and p_{ivc} from 99.5 kPa to 113.3 kPa. Measurements from the

[3] T_{ivc} is difficult to measure and depending on the thermal condition of an engine, an increase or decrease in the mixture temperature between valve opening to IVC may occur.

Ricardo engine are taken at two engine speeds with two PRFs[4] (20PRF and 10PRF). Furthermore, two valve timings are run to test the performance of the model when valve timing is changed. (With lower compression ratio of the Ricardo engine, auto ignition is more easily obtained for the case of earlier IVC, as p_{ivc} is higher in this case.)

Figures 7 compares three samples pressure histories determined by the thermokinetic model with 50-cycle average pressure traces measured in the Ricardo engine. The simulated and measured pressure traces are in good agreement. As expected, simulations have higher peak pressures than those of experimental traces. This is inherent to the single zone model where it is assumed that the entire mixture is uniform in temperature, pressure and composition and it ignites and combusts concurrently. Blow-by is ignored and it is also assumed that all of the fuel reacts. These are clearly simplifications for a real engine and they lead to having higher total heat release and exothermicity in single zone simulations. An engine model using the single zone assumption can be interpreted as an engine with higher efficiency, leading to higher pressure after the ignition. Combustion durations predicted by the single zone model are shorter than those observed in the experiments, which has also been noted elsewhere (Aceves et al. 2000).

The calculated and simulated ignition timings for all ten cases listed in Table 5 are compared in Table 6. The experimental ignition timings are again taken from 50 consecutive engine cycles. As shown in Table 6, all predicted ignition timings are within the range of experimental data except for tests #8 and #5 where ignition is predicted to occur 0.3 and 0.7 CAD later than the measured range respectively. A maximum deviation of 0.7 CAD between the simulation and the experiment indicates that the thermokinetic model can be used to predict ignition delay, despite the simplified assumptions.

To re-iterate, the purpose of this model was not to predict the absolute ignition delays, rather only to capture the qualitative influences of different engine parameters, which, as shown by Tables 4 and 6, has been accomplished. The thermokinetic model is capable of predicting the qualitative trends of the ignition timing, something which is critical for future work in designing control strategies for HCCI combustion.

[4] As the compression ratio of Ricardo engine is not high, it doesn't run under HCCI mode with high octane number fuel. Therefore running Ricardo engine under HCCI mode is possible only with lower PRF blends (i.e. lower iso-octane fraction). 20PRF was the highest PRF blend for which HCCI operation was possible with the Ricardo engine.

4 Conclusions

A one zone thermokinetic model using a chemical kinetic mechanism for primary reference fuels is developed and validated using a step by step methodology. A new kinetic mechanism is formed by combining the ignition, and intermediate and high temperature sub-mechanisms, of Zheng et al. (2002) with the H_2/O_2 mechanism of Marinov et al. (1995). The ability of the model to predict the thermodynamic equilibrium state after a constant volume combustion event is validated using STANJAN. It was found that the temperature and concentrations of major exhaust products could be predicted to within 8.5%.

The ability of the model to predict ignition delays is validated using experimental measurements first from a rapid compression machine (RCM) and then from a shock tube. From these two investigations it is shown that the thermokinetic model is capable of predicting ignition delays in practical combustion systems that have different fuel octane numbers, equivalence ratios and initial temperatures and pressures.

As the intended application of this model is the prediction of autoignition in an HCCI engine, experimentally measured HCCI pressure traces are compared to those calculated by the thermokinetic model. Two different engines are used to assess the performance of the model over a range of intake temperatures, equivalence ratios, EGR rates, initial pressures, and valve timings. Three different engine speeds and four different PRF blends are considered. Through this extensive evaluation, the model was able to predict the start of ignition within a maximum error of 1.7 CAD from the range of experimental measurements.

The primary goal of the thermokinetic model, to predict the qualitative effect of engine parameters on the autoignition timing in a HCCI engine, is achieved. It is considered acceptable that the one zone thermokinetic model is not capable of accurately predicting phenomena after ignition, such as emissions, peak combustion pressure, and combustion duration, as the objective is to predict ignition timing without excessive computational requirements.

To predict post-ignition phenomena this model must be extended to a multi-zone model, in which spatial variations of the thermodynamic state are included. This extended thermodynamic model should more accurately predict the post-ignition phenomena, at the expense of higher computational requirements.

5 Acknowledgements

Financial support received from the Natural Sciences and Engineering Research Council of Canada (NSERC) research grant number 249553-02 and Canadian Federal Networks of Centers of Excellence (NCE) program under AUTO21 research grant D01-DAF/DO5 is acknowledged. The authors would also like to acknowledge the Westgrid High Performance Computing network which was used to obtain many of the results presented in this paper. Finally, the comments and suggestions provided by Dr. Larry Kostiuk are most gratefully acknowledged.

References

Aceves, S. M., Flowers, D. L., Westbrook, C. K., Smith, J. R., Pitz, W., Dibble, R., Christensen, M. and Johansson, B. (2000) A Multi-zone Model for Prediction of HCCI Combustion and Emissions. SAE 2000-01-0327.

Atkins, M. (2004) Experimental Examination of the Effects of Fuel Octane and Diluent on HCCI Combustion, M.Sc. Thesis, University of Alberta.

Atkins, M. and Koch, C. R. (2005) The Effect of Fuel Octane and Diluent on HCCI Combustion. Proceeding of IMechE - Part D 219, 665 – 675.

Benson, S. W. (1976) Thermochemical Kinetics, 2nd Ed., Wiley, New York.

Burcat, A. (1984) Thermochemical Data for Combustion Calculations, in W. C. Gardiner (ed.), Combustion Chemistry, Springer-Verlag, New York, pp. 455–473.

Burcat, A. (2001) Third Millenium Ideal Gas and Condensed Phase Thermochemical Database for Combustion, Technical Report TAE 867, Faculty of Aerospace Engineering, Israel Institute of Technology.

Chang, J., Guralp, O., Filipi, Z., Assanis, D., Kuo, T., Najt, P. and Rask, R. (2004) New Heat Transfer Correlation for an HCCI Engine Derived From Measurements of Instantaneous Surface Heat Flux. SAE 2004-01-2996.

Checkel, M. D. and Dale, J. D. (1986) Computerized Knock Detection from Engine Pressure Records. SAE 860028.

Come, G.-M. (2001) Gas-Phase Thermal Reactions : Chemical Engineering Kinetics, Kluwer Academic

Publishers, Boston.

Curran, H. J., Gaffuri, P., Pitz, W. J. and Westbrook, C. K. (1998) A Comprehensive Modeling Study of n-heptane Oxidation, Combustion and Flame 114(1-2), 149–177.

Curran, H. J., Gaffuri, P., Pitz, W. J. and Westbrook, C. K. (2002) A Comprehensive Modeling Study of iso-octane Oxidation, Combustion and Flame 129(3), 253–280.

Fiveland, S. B. and Assanis, D. N. (2000) A Four-Stroke Homogeneous Charge Compression Ignition Engine Simulation for Combustion and Performance Studies. SAE 2000-01-0332.

Gauthier, B. M., Davidson, D. F. and Hanson, R. K. (2004) Shock Tube Determination of Ignition Delay Times in Full-blend and Surrogate Fuel Mixtures, Combustion and Flame 139, 300–311.

Glassman, I. (1996) Combustion, 3rd Ed., Academic Press, San Diego, Calif.

Griffiths, J. F., Hughes, K. J., Schreiber, M. and Poppe, C. (1994) A Unified Approach to the Reduced Kinetic Modeling of Alkane Combustion, Combustion and Flame 99(3-4), 533–540.

Griffiths, J. F., Jiao, Q., Kordylewski, W., Schreiber, M., Meyer, J. and Knoche, K. F. (1993) Experimental and Numerical-Studies of Ditertiary Butyl Peroxide Combustion at High-Pressures in a Rapid Compression Machine, Combustion and Flame 93(3), 303–315.

Kirchen, P. (2004) Thermodynamic Modeling of the HCCI Cycle: Predicting the Ignition Timing, M.Sc. Thesis, University of Alberta.

Halstead, M. P., Kirsch, L. J. and Quinn, C. P. (1977) Autoignition of Hydrocarbon Fuels at High Temperatures and Pressures - Fitting of a Mathematical Model, Combustion and Flame 30(1), 45–60.

Hu, H. and Keck, J. (1987) Autoignition of Adiabatically Compressed Combustible Gas Mixtures. SAE 872110.

Lavy, J., Dabadie, J.-C., Angelberger, C., Duret, P., Juretzka, A., Schaflein, J., Ma, T. H., Lendresse, Y., Satre, A., Schulz, C., Krmer, H., Zhao, H.and Damiano, L. (2000) Innovative Ultra-low NOx Controlled Auto-Ignition Combustion Process for Gasoline Engines: the 4-SPACE Project. SAE 2000-01-1837.

Li, H., Miller, David, L. and Cernansky, N. P. (1996) Development of a Reduced Chemical Kinetic Model for Prediction of Preignition Reactivity and Autoignition of Primary Reference Fuels. SAE 960498.

Marinov, N. M., Westbrook, C. K. and Pitz, W. J. (1995) Detailed and Global Chemical Kinetics Model

for Hydrogen, Transport Phenomena in Combustion: Proceeding of the Eighth International Symposium on Transport Phenomena, Taylor and Francis, San Francisco, California, USA, pp. 118–130.

Najt, P. M. and Foster, D. E. (1983) Compression-ignited Homogeneous Charge Combustion. SAE 830264.

Onishi, S., Jo, S. H., Shoda, K., Jo, P. D. and Kato, S. (1979) Active Thermo-Atmosphere Combustion (ATAC) a New Combustion Process for Internal Combustion Engines. SAE 790501.

Park, P. and Keck, J. C. (1990) Rapid Compression Machine Measurements of Ignition Delays for Primary Reference Fuels. SAE 900027.

Reynolds, W. (1987) STANJAN Chemical Equilibrium Solver. v3.91, IBM-PC.

Slavinskaya, N. A. and Haidn, O. J. (2003) Modeling of n-heptane and iso-octane Oxidation in Air, Journal of Propulsion and Power 19(6), 1200–1216.

Smith, G., Golden, D., Frenklach, M., Moriarty, N., Eiteneer, B., Goldenberg, M., Bowmann, C., Hanson, R., Song, S., Gardiner, W. C., Lissianski, V. V. and Qin, Z.: 2004, GRI-Mech 3.0. http://www.me.berkeley.edu/gri-mech/version30/text30.html.

Stein, S. E. and Brown, R. L. (2003) Structures and Properties Group Additivity Model, in P. J. Linstrom and W. G. Mallard (eds), NIST Chemistry WebBook, NIST Standard Reference Database Number 69, National Institute of Standards and Technology, Gaithersburg MD, 20899. http://webbook.nist.gov.

Tanaka, S., Ayala, F. and Keck, J. C. (2003) A Reduced Chemical Kinetic Model for HCCI Combustion of Primary Reference Fuels in a Rapid Compression Machine, Combustion and Flame 133(4), 467–481.

Tunest˚al, P., Olsson, J. and Johansson, B. (2002) Closed Loop Control of HCCI Engines, in R. Johansson and A. Rantzer (eds), Nonlinear and Hybrid Systems in Automotive Control, Springer-Verlag, Lund.

Warnatz, J. (2000) Hydrocarbon Oxidation High-temperature Chemistry, Pure and Applied Chemistry 72(11), 2101–2110.

Woschni, G. (1967) Universally Applicable Equation for the Instantaneous Heat Transfer Coefficient in the Internal Combustion Engine. SAE 670931.

Zheng, J., Yang, W., Miller, D. L. and Cernansky, N. P. (2002) A skeletal chemical kinetic model for the HCCI combustion process. SAE 2002-01-0423.

Table 1: Compression conditions used for RCM validation. Ignition delay is determined for stoichio-metric mixtures of 0, 50, 75, 90, and 100 PRF blends (Park and Keck 1990).

Temperature [K]	Pressure [kPa]
760	5769
752	2941
732	5581
720	2829
686	5166
672	2569

Table 2: Configurations of the CFR and Ricardo single-cylinder engines. IVC: Intake Valve Closing, EVO: Exhaust Valve Opening, aBDC: after Bottom Dead Center.

Parameters	CFR engine	Ricardo engine[5]
Bore × Stroke [mm]	83 × 114	80 × 88.9
Compression Ratio	12	10
Displacement [L]	0.622	0.447
Number of Valves	2	4
IVC [aBDC]	34˚	60˚
EVO [aBDC]	- 40˚	-70˚

Table 3: Engine operating conditions for HCCI validation using the CFR engine. All points at N =700rpm, Indicated Mean Effective Pressure ≈ 5bar. T_{in}: intake temperature, p_{ivc}: cylinder pressure at IVC.

PRF	Φ	EGR [%]	T_{in} [K]	p_{ivc} [kPa]
20	0.983	30.5	360	94.1
40	0.808	18.9	360	90.0
60	0.662	1.42	360	90.2

[5] Two experimental set-ups are used for the Ricardo engine. These two set-ups only differ in valve timings. Both intake and exhaust valves in the second configuration open and close 5 degrees before the values given in Table 2 (the first configuration).

Table 4: Comparison of the experimental ignition timing (Atkins 2004) and those determined using the thermokinetic model. CAD aTDC: Crank Angle Degrees after Top Dead Center.

Fuel (PRF)	Ignition Timing [CAD aTDC]	
	Experiment	Simulation
20	-0.6 → 2.7	-2.3
40	-1.1 → 1.8	0.7
60	-0.1 → 3.7	1.8

Table 5: Engine operating conditions for the HCCI validation using the Ricardo engine.

Test No.	Fuel [PRF]	IVC [aBDC]	N [rpm]	Φ	*EGR*	$T_{in}[K]$	p_{ivc} [kPa]
1	10	55°	800	0.47	1.21	127	106.4
2	10	55°	800	0.53	1.18	144	105.7
3	10	55°	800	0.67	6.02	79	105.3
4	10	55°	800	0.8	19.10	82	113.3
5	20	55°	1000	0.65	2.1	110	105.4
6	20	55°	1000	0.66	0	113	107.7
7	20	55°	1000	0.76	8.4	58	109.8
8	20	60°	800	0.67	1	120	102.5
9	20	60°	800	0.71	0	120	101.6
10	20	60°	800	0.83	10	112	99.5

Table 6: Comparison of the measured and simulated ignition timings for the Ricardo engine.

Test No.	Ignition Timing [CAD aTDC]	
	Experiment	Simulation
1	7.5 → 11.6	11.2
2	2.6 → 8.8	6.7
3	7.4 → 9.9	9.8
4	8.9 → 13.6	10.9
5	3.7 → 5.4	6.1
6	5.2 → 8.5	5.8
7	13 → 16.7	16.3
8	7.5 → 9.4	9.7
9	10.2 → 12.3	10.7
10	11 → 16.2	13

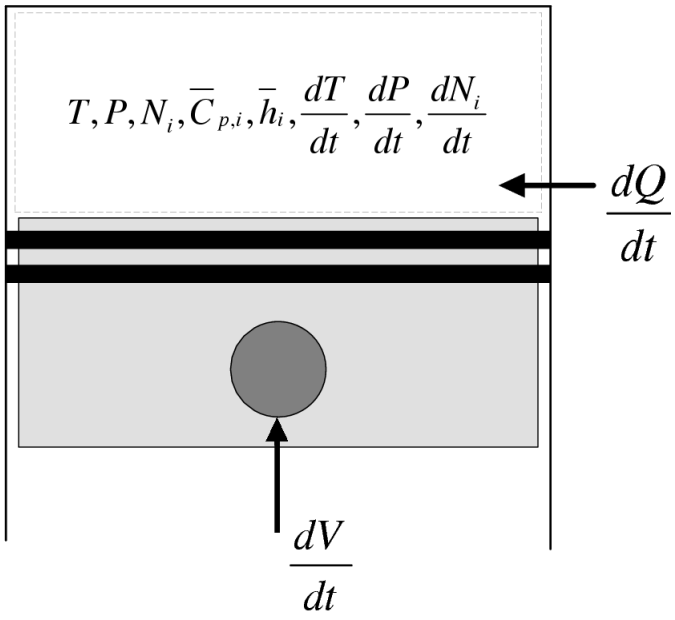

Figure 1: Single zone control volume used in the first law analysis.

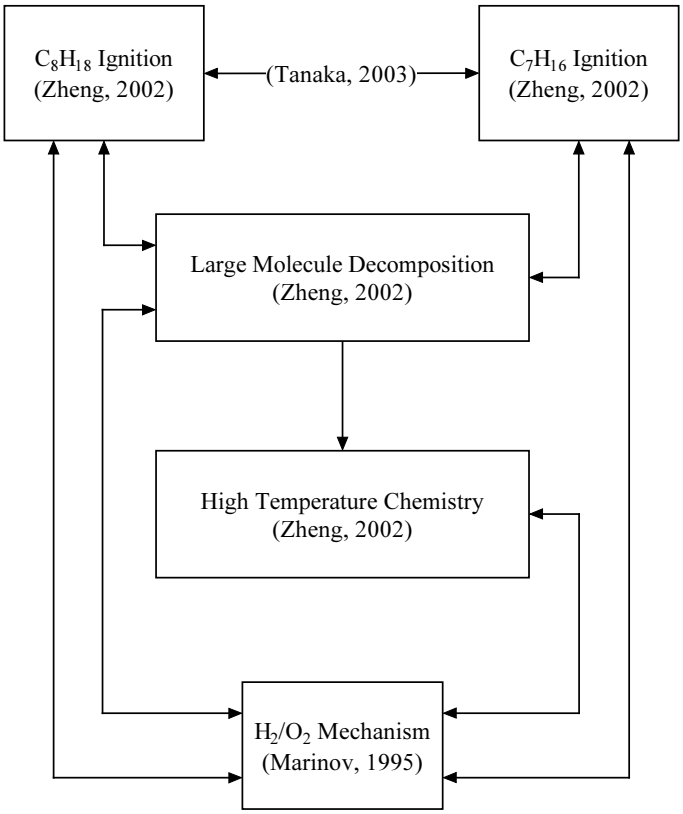

Figure 2: Schematic of the reduced chemical kinetics model of n-heptane and iso-octane mixtures

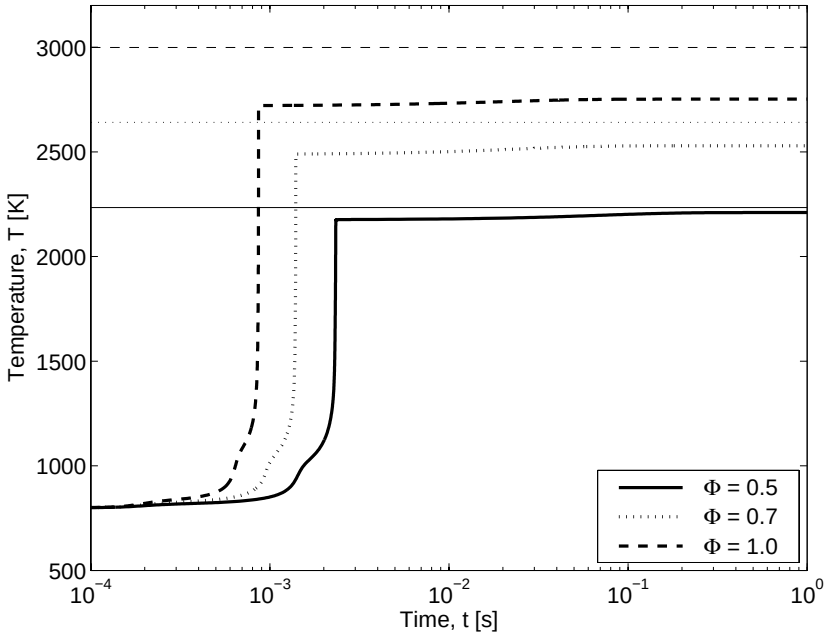

Figure 3: Comparison of constant volume, adiabatic combustion temperatures calculated using the thermokinetic mechanism and STANJAN. Horizontal lines indicate equilibrium temperatures predicted by STANJAN. 20PRF, $T_o = 800K$, $P_o = 30bar$.

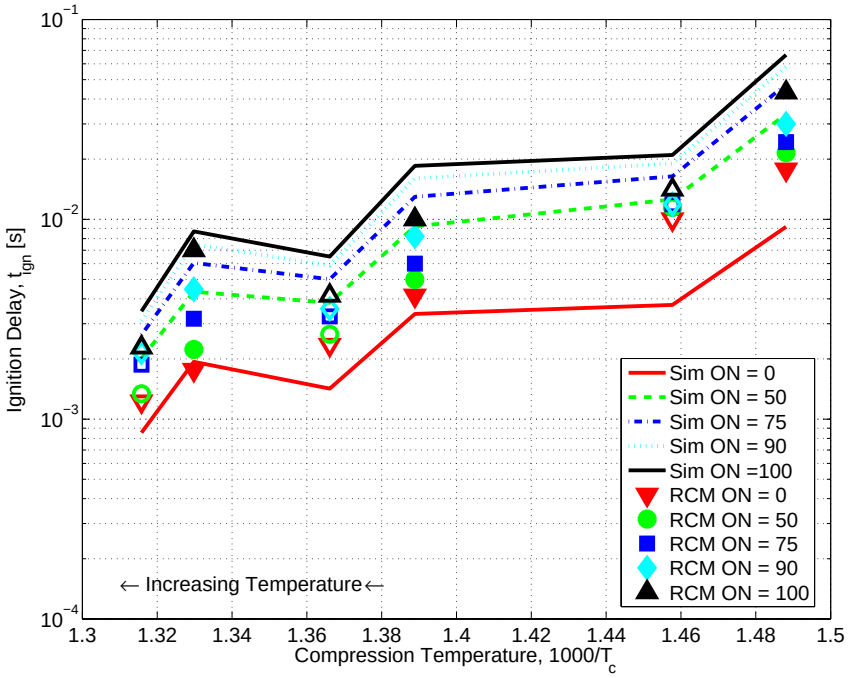

Figure 4: Observed and calculated ignition delays in a RCM for various PRFs. Initial conditions for each simulation are given in Table 1. Solid markers indicate compression pressures of ≈ 2MPa and hollow markers indicate compression pressures of ≈ 4MPa. Experimental ignition delays from Park and Keck (1990)

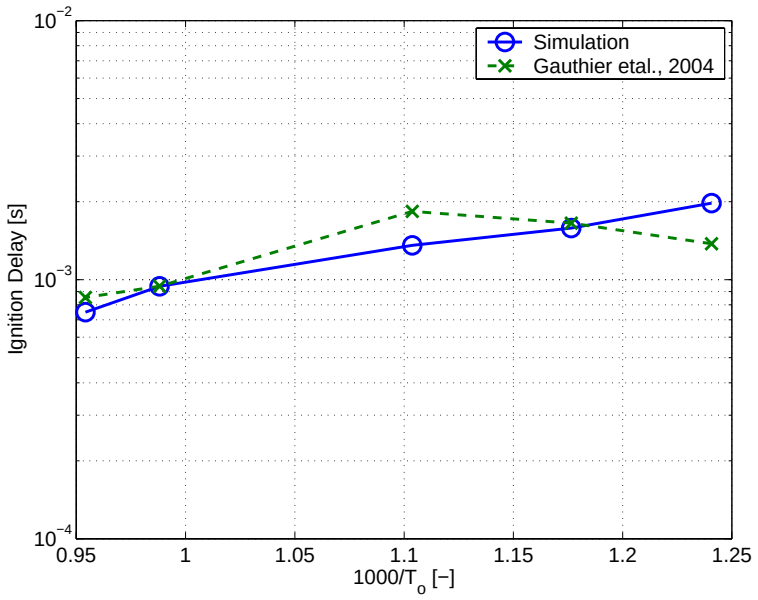

Figure 5: Comparison of experimental and simulation shock tube ignition delays for n-heptane. Φ = 1.0, EGR=0%, P_o = 20bar, experimental data taken from Gauthier et al. (2004).

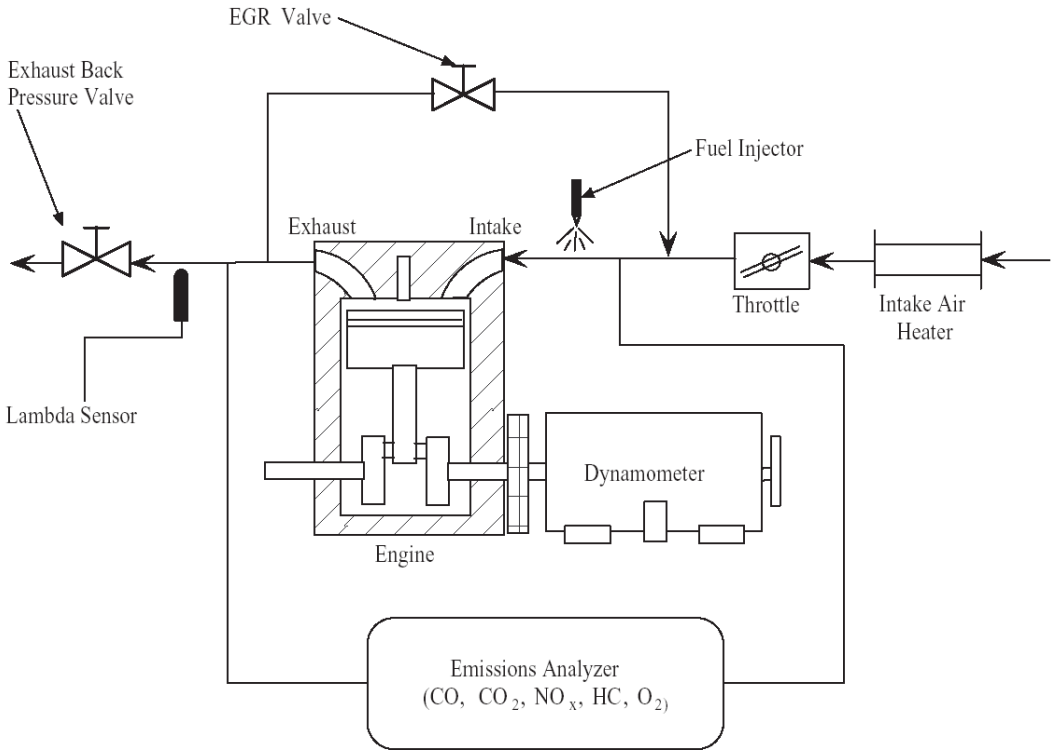

Figure 6: General schematic of the testbench used to obtain experimental data for HCCI validation. (with both the CFR and Ricardo engine)

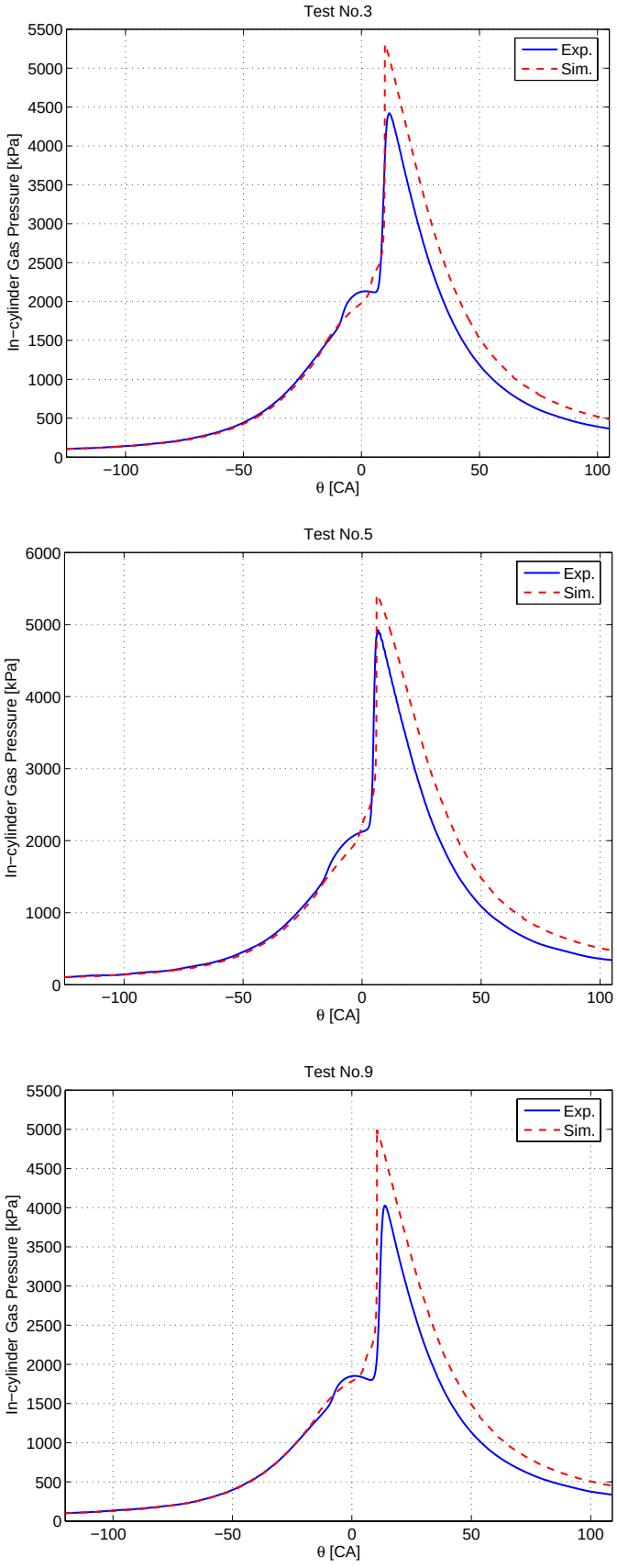

Figure 7: Comparison of simulated and experimental pressure histories for three sample conditions given in Table 5.

Table 7: Reactions of the kinetic mechanism shown in Figure 2. "↔" separator indicates that the reactants and products are in equilibrium. References: [1](Zheng et al. 2002), [2] (Li et al. 1996), [3] (Tanaka et al. 2003), [4] (Marinov et al. 1995), [5] (Smith et al. 2004). Units: kcal, mol, cm^3, s

#	Reaction	log(A)	n	E_a	Source
1	$C_8H_{18} + O_2 \rightarrow C_8H_{17} + HO_2$	16	0	46	[1]
2	$C_8H_{17} + HO_2 \rightarrow C_8H_{18} + O_2$	12	0	0	[1]
3	$C_8H_{17} + O_2 \rightarrow C_8H_{17}OO$	12	0	0	[1]
4	$C_8H_{17}OO \rightarrow C_8H_{17} + O_2$	13.4	0	27.4	[1]
5	$C_8H_{17}OO \rightarrow C_8H_{16}OOH$	11	0	22.4	[2]
6	$C_8H_{16}OOH \rightarrow C_8H_{17}OO$	11	0	11	[2]
7	$C_8H_{16}OOH + O_2 \rightarrow OOC_8H_{16}OOH$	11.5	0	0	[1]
8	$OOC_8H_{16}OOH \rightarrow C_8H_{16}OOH + O_2$	13.4	0	27.4	[1]
9	$OOC_8H_{16}OOH \rightarrow OC_8H_{15}OOH + OH$	11.3	0	17	[1]
10	$OH + C_8H_{18} \rightarrow H_2O + C_8H_{17}$	13.3	0	3	[1]
11	$OC_8H_{15}OOH \rightarrow OC_8H_{15}O + OH$	15.6	0	40	[1]
12	$OC_8H_{15}O \rightarrow HCHO + C_3H_7CHO + C_3H_5$	14	0	15	[1]
13	$C_8H_{16}OOH \rightarrow C_3H_7CHO + OH + C_4H_8$	14.4	0	31	[1]
14	$C_8H_{17}OO + C_3H_7CHO \rightarrow C_8H_{17}OOH + C_3H_7CO$	11.4	0	8.6	[1]
15	$HO_2 + C_8H_{18} \rightarrow C_8H_{17} + H_2O_2$	11.7	0	16	[1]
16	$C_8H_{17} + H_2O_2 \rightarrow HO_2 + C_8H_{18}$	10.8	0	8	[1]
17	$C_8H_{17}OO + C_8H_{18} \rightarrow C_8H_{17}OOH + C_8H_{17}$	11.2	0	16	[1]
18	$C_8H_{17}OOH + C_8H_{17} \rightarrow C_8H_{17}OO + C_8H_{18}$	10.1	0	8	[1]
19	$C_8H_{18} + C_3H_7O_2 \rightarrow C_3H_7OOH + C_8H_{17}$	11.3	0	16	[1]
20	$C_3H_7OOH + C_8H_{17} \rightarrow C_8H_{18} + C_3H_7O_2$	10.1	0	8	[1]
21	$C_8H_{16} + OH + O_2 \rightarrow OH + 2C_3H_7CHO$	12.8	0	-1.04	[1]
22	$C_8H_{17}OOH \rightarrow C_8H_{17}O + OH$	15.6	0	43	[1]
23	$C_8H_{17}O \rightarrow C_4H_9 + C_3H_7CHO$	13.3	0	15	[1]
24	$C_8H_{17}OO \rightarrow C_8H_{16} + HO_2$	9.85	0	23	[1]
25	$C_8H_{17}OO \rightarrow C_8H_{16}O + OH$	8.78	0	18	[2]
26	$C_8H_{16}O \rightarrow CH_3O + C_7H_{13}$	14.7	0	24.8	[1]
27	$C_7H_{16} + O_2 \rightarrow C_7H_{15} + HO_2$	16	0	46	[1]
28	$C_7H_{15} + HO_2 \rightarrow C_7H_{16} + O_2$	13.8	0	0	[1]
29	$C_7H_{15} + O_2 \rightarrow C_7H_{15}OO$	12	0	0	[1]
30	$C_7H_{15}OO \rightarrow C_7H_{15} + O_2$	13.4	0	27.4	[1]
31	$C_7H_{15}OO \rightarrow C_7H_{14}OOH$	11.9	0	19	[2]
32	$C_7H_{14}OOH \rightarrow C_7H_{15}OO$	11	0	11	[2]
33	$C_7H_{14}OOH + O_2 \rightarrow OOC_7H_{14}OOH$	11.5	0	0	[1]
34	$OOC_7H_{14}OOH \rightarrow C_7H_{14}OOH + O_2$	13.4	0	27.4	[1]
35	$OOC_7H_{14}OOH \rightarrow OC_7H_{13}OOH + OH$	11.3	0	17	[1]
36	$OH + C_7H_{16} \rightarrow H_2O + C_7H_{15}$	13	0	3	[1]
37	$OC_7H_{13}OOH \rightarrow OC_7H_{13}O + OH$	15.6	0	40	[1]
38	$OC_7H_{13}O \rightarrow HCHO + C_3H_7CHO + C_2H_3$	14	0	15	[1]
39	$C_7H_{14}OOH \rightarrow C_3H_7CHO + OH + C_3H_6$	14.4	0	31	[1]
40	$C_7H_{15}OO + C_3H_7CHO \rightarrow C_7H_{15}OOH + C_3H_7CO$	11.4	0	8.6	[1]
41	$HO_2 + C_7H_{16} \rightarrow C_7H_{15} + H_2O_2$	11.7	0	16	[1]
42	$C_7H_{15} + H_2O_2 \rightarrow HO_2 + C_7H_{16}$	10.8	0	8	[1]

Continued on next page …

43	C7H15OO + C7H16 → C7H15OOH + C7H15	11.2	0	16	[1]
44	C7H15OOH + C7H15 → C7H15OO + C7H16	10.1	0	8	[1]
45	$C_7H_{16} + C_3H_7O_2 \rightarrow C_3H_7OOH + C_7H_{15}$	11.3	0	16	[1]
46	$C_3H_7OOH + C_7H_{15} \rightarrow C_7H_{16} + C_3H_7O_2$	10.1	0	8	[1]
47	$C_7H_{15}OOH \rightarrow C_7H_{15}O + OH$	15.6	0	43	[1]
48	$C_7H_{15}O \rightarrow C_3H_7 + C_3H_7CHO$	13.3	0	15	[1]
49	$C_7H_{15}OO \rightarrow C_7H_{14} + HO_2$	9.85	0	23	[1]
50	$C_7H_{15}OO \rightarrow C_7H_{14}O + OH$	9.48	0	18	[2]
51	$C_7H_{14} + OH + O_2 \rightarrow OH + C_3H_7CHO + C_2H_5CHO$	12.7	0	-1.04	[1]
52	$C_7H_{14}O \rightarrow CH_3O + C_6H_{11}$	14.7	0	24.8	[1]
53	$HO_2 + C_3H_7CHO \rightarrow H_2O_2 + C_3H_7CO$	11.7	0	8.64	[1]
54	$C_3H_6 + HO_2 \rightarrow C_3H_6O + OH$	10.9	0	10	[1]
55	$C_4H_8 + HO_2 \rightarrow C_4H_8O + OH$	10.9	0	10	[1]
56	$C_3H_7CHO + OH \rightarrow C_3H_7CO + H_2O$	13.3	0	0	[1]
57	$C_3H_7CO + M \rightarrow M + CO + C_3H_7$	16.8	0	15	[1]
58	$C_3H_7 + O_2 \rightarrow C_3H_7O_2$	12	0	0	[1]
59	$C_3H_7O_2 \rightarrow C_3H_7 + O_2$	13.4	0	27.4	[1]
60	$C_3H_7O_2 \rightarrow C_3H_6 + HO_2$	11.8	0	28.9	[1]
61	$C_3H_7CHO + C_3H_7O_2 \rightarrow C_3H_7OOH + C_3H_7CO$	11.5	0	8.6	[1]
62	$C_3H_7OOH \rightarrow C_3H_7O + OH$	15.6	0	43	[1]
63	$C_3H_7O + O_2 \rightarrow C_3H_6O + HO_2$	10.6	0	2.14	[1]
64	C8H18 +C7H15 ↔ C7H16 +C8H17	12.7	0	0	[3]
65	$C_3H_6O \rightarrow C_2H_5 + HCO$	13.3	0	57.2	[1]
66	$C_4H_8O \rightarrow C_3H_7 + HCO$	13.3	0	57.2	[1]
67	$C_3H_7CHO + M \rightarrow M + C_3H_7 + HCO$	15.9	0	81.8	[1]
68	$C_4H_9 \rightarrow CH_3 + C_3H_6$	13.4	0	31.9	[1]
69	$C_6H_{11} \rightarrow C_2H_4 + C_4H_7$	11	0	37.1	[1]
70	$C_7H_{13} \rightarrow C_3H_4 + C_4H_9$	11	0	37.1	[1]
71	$C_4H_7 \rightarrow C_2H_4 + C_2H_3$	11	0	37.1	[1]
72	$C_2H_5CHO + M \rightarrow M + C_2H_5 + HCO$	15.9	0	81.8	[1]
73	$OH + H_2 \leftrightarrow H + H_2O$	8.33	1.52	3.45	[4]
74	$O + OH \leftrightarrow O_2 + H$	14.3	-0.4	0	[4]
75	$O + H_2 \leftrightarrow OH + H$	4.7	2.67	6.29	[4]
76[10]	$H + O_2 \leftrightarrow HO_2$	13.7	0	0	[4]
	low pressure...	19	-1.26	0	
77	$H + O_2 + N_2 \leftrightarrow N_2 + HO_2$	13.7	0	0	[4]
	low pressure...	20.3	-1.59	0	
78	$H + O_2 + H_2 \leftrightarrow H_2 + HO_2$	13.7	0	0	[4]
	low pressure...	19.2	-1.13	0	
79	$H + O_2 + H_2O \leftrightarrow H_2O + HO_2$	13.7	0	0	[4]
	low pressure...	23.3	-2.44	0	
80	$OH + HO_2 \leftrightarrow H_2O + O_2$	13.5	0	-0.5	[4]
81	$H + HO_2 \leftrightarrow 2OH$	14.2	0	1	[4]
82	$H + HO_2 \leftrightarrow H_2 + O_2$	11.9	0.65	1.24	[4]
83	$H + HO_2 \leftrightarrow O + H_2O$	13.5	0	1.72	[4]
84	$O + HO_2 \leftrightarrow O_2 + OH$	13.5	0	0	[4]
85	$2OH \leftrightarrow O + H_2O$	4.55	2.4	-2.11	[4]

Continued on next page …

[10] Third body efficiencies: H_2O, 0; H_2, 0; N_2, 0;

86[11]	$2H + M \leftrightarrow M + H_2$	18	-1	0	[4]
87	$2H + H_2 \leftrightarrow 2H_2$	17	-0.6	0	[4]
88	$2H + H_2O \leftrightarrow H_2O + H_2$	19.8	-1.25	0	[4]
89[12]	$H + OH + M \leftrightarrow M + H_2O$	22.3	-1.25	0	[4]
90	$H + O + M \leftrightarrow M + OH$	18.7	-1	0	[4]
91	$2O + M \leftrightarrow M + O_2$	13.3	0	-1.79	[4]
92	$2HO_2 \leftrightarrow H_2O_2 + O_2$	14.6	0	12	[4]
93	$2HO_2 \leftrightarrow H_2O_2 + O_2$	11.1	0	-1.63	[4]
94	$2OH \leftrightarrow H_2O_2$	14.1	-0.37	0	[4]
	low pressure...	30.5	-4.63	2.05	
95	$H_2O_2 + H \leftrightarrow OH + H_2O$	13.5	0	4.22	[4]
96	$H_2O_2 + H \leftrightarrow HO_2 + H_2$	6.3	2	2.44	[4]
97	$H_2O_2 + O \leftrightarrow OH + HO_2$	6.98	2	3.97	[4]
98	$H_2O_2 + OH \leftrightarrow H_2O + HO_2$	0.38	4.04	-2.16	[4]
99	$CO + OH \leftrightarrow CO_2 + H$	7.68	1.23	0.07	[5]
100	$CO + HO_2 \leftrightarrow CO_2 + OH$	14.2	0	23.6	[5]
101[13]	$CO + O \leftrightarrow CO_2$	10.3	0	2.39	[5]
	low pressure...	14.8	0	3	
102	$CO + O_2 \leftrightarrow CO_2 + O$	12.4	0	47.8	[5]
103	$HCO + O_2 \rightarrow CO + HO_2$	13.1	0	0.4	[1]
104	$HCO + M \rightarrow M + CO + H$	17.3	-1	17	[1]
105	$HCHO + O \rightarrow HCO + OH$	13.6	0	3.54	[1]
106	$HCHO + OH \rightarrow HCO + H_2O$	9.54	1.2	-0.45	[1]
107	$HCHO + HO_2 \rightarrow HCO + H_2O_2$	6.75	2	12	[1]
108	$HCHO + O_2 \rightarrow HCO + HO_2$	14	0	40	[1]
109	$CH_3 + O_2 \rightarrow HCHO + OH$	12.4	0	20.3	[1]
110	$C_2H_3 + O_2 \rightarrow HCHO + HCO$	12.6	0	-0.25	[1]
111	$C_2H_4 + OH \rightarrow C_2H_3 + H_2O$	6.56	2	2.5	[1]
112	$C_2H_4 + O \rightarrow CH_3 + HCO$	7.1	1.8	0.22	[1]
113	$C_2H_5 + O_2 \rightarrow C_2H_4 + HO_2$	11.9	0	3.88	[1]
114	$C_3H_5 + O_2 \rightarrow C_3H_4 + HO_2$	11.8	0	10	[1]
115	$C_3H_4 + OH \rightarrow HCHO + C_2H_3$	12	0	0	[1]
116	$C_3H_6 + OH \rightarrow C_3H_5 + H_2O$	6.49	2	-0.3	[1]
117	$C_3H_6 + O_2 \rightarrow C_3H_5 + HO_2$	12.3	0	39	[1]
118	$C_3H_6 + HO_2 \rightarrow C_3H_5 + H_2O_2$	11.5	0	14.9	[1]
119	$C_3H_7 \rightarrow C_2H_4 + CH_3$	10.3	0	29.5	[1]
120	$CH_3O + O_2 \underline{\rightarrow} HCHO + HO_2$	10.9	0	2.7	[1]

[11] Third body efficiences: H_2O, 0; H_2, 0;

[12] Third body efficiences: H_2O, 6.3;

[13] Third body efficiences: H_2, 2; O_2, 6; H_2O, 6; CO, 1.5; CO_2, 3.5;